MICROWAVE AND FAR INFRARED DIAGNOSTICS

A. Krämer-Flecken
Institut für Plasmaphysik, Forschungszentrum Jülich
Association EURATOM-FZJ, Trilateral Euregio Cluster, D-52425, Jülich, Germany

I. INTRODUCTION

The measurement of plasma quantities is a difficult task since the plasma cannot be treated like normal material. Any measurement of plasma quantities with electrostatic probes will yield interactions with the plasma and causes a perturbation of the measured quantity. Inside a hot plasma those methods are not applicable, since they may lead to a disruption of the discharge.
Other ways of diagnosing a hot plasma are the measurement of the emitted radiation in the infrared and microwave region as well as the probing of the plasma with infrared and micro waves. The measurement of the optical properties (e.g. refractive index) yields also information about the plasma. With microwave and far infrared diagnostics plasma properties can be measured quite accurate and reliable. Main plasma parameters as the electron density and the electron temperature can be measured. Even the measurement of fluctuations in density and temperature and the determination of the plasma current density are possible with sophisticated diagnostics.
In the following section the optical properties of the plasma will be developed. The sections III to VI are devoted to different diagnostic techniques.

II. PROPAGATION OF WAVES IN A COLD PLASMA - THE DISPERSION RELATION

All microwave and far infrared diagnostics are based on the measurement of emitted radiation from the plasma and its propagation within the plasma, or of the propagation of externally launched microwaves and far infrared radiation through the plasma. This means the optical properties of a plasma have to be measured in detail. Specially the refractive index of the plasma will be of great importance. It tells us whether the incident waves will be absorbed or reflected in the plasma. The propagation of electromagnetic radiation within the plasma is described by Maxwells equations [1].

$$\nabla \times \mathbf{E} = -\frac{\partial \mathbf{B}}{\partial t} \quad ; \quad \nabla \times \mathbf{B} = \mu_0 \mathbf{j} + \epsilon_0 \mu_0 \frac{\partial \mathbf{E}}{\partial t} \qquad (1)$$

After eliminating $\mathbf{B}$ we will get a differential equation for $\mathbf{E}$

$$\nabla \times (\nabla \times \mathbf{E}) + \frac{\partial}{\partial t}\left(\mu_0 \mathbf{j} + \epsilon_0 \mu_0 \frac{\partial \mathbf{E}}{\partial t}\right) = 0 \qquad (2)$$

Taking into account the superposition principle we can decompose the equation into a time dependent part and a frequency dependent part by using Fourier transformation for the electric field as

$$\mathbf{E}(x,t) = \int E(\mathbf{k},\omega)\, e^{-i(k\ x-\omega\ t)} d^3\mathbf{k}\ dt. \qquad (3)$$

Inserting the above equation into Eq. 2 we obtain

$$\mathbf{k} \times (\mathbf{k} \times \mathbf{E}) + i\omega\left(\mu_0 \sigma \cdot \mathbf{E} - i\omega\epsilon_0\mu_0 \mathbf{E}\right) = 0 \qquad (4)$$

where $\mathbf{k}$ is the wave vector of the Fourier mode. The current density was expressed as $\mathbf{j} = -en_e\mathbf{v_e} = \boldsymbol{\sigma} \cdot \mathbf{E}$, ($\boldsymbol{\sigma}$ is the conductivity tensor of the plasma). Nonzero solutions for $\mathbf{E}$ can be found if the determinant of the coefficient matrix is zero.

$$det\left|\mathbf{kk} - k^2 \cdot \mathbf{1} + \frac{\omega^2}{c^2} \cdot \boldsymbol{\epsilon}\right| = 0 \qquad (5)$$

The above equation is called the dispersion relation, relating wave vectors with the frequency. $\boldsymbol{\epsilon}$ denotes the dielectric tensor.

$$\boldsymbol{\epsilon} = \left(\mathbf{1} + \frac{i}{\omega\epsilon_0}\boldsymbol{\sigma}\right) \qquad (6)$$

For an isotropic plasma the refractive index N is related to the dielectric tensor ϵ by

$$N = \frac{kc}{\omega} = \epsilon^{1/2} \qquad (7)$$

From Eq. 5 we can obtain the *Appleton–Hartree* formula for the refractive index of the plasma. To achieve this equation we first have to calculate the conductivity σ in Eq. 6 from the equation of motion of charged particles within the plasma which is given by

$$m_e \frac{\partial \mathbf{v_e}}{\partial t} = -e\left(\mathbf{E} + \mathbf{v_e} \times \mathbf{B}\right) \qquad (8)$$

Hereby we assumed that the electrons due to the smaller mass m_e have the larger mobility and the ions are mostly at rest. For a Cartesian coordinate system with the magnetic field along the z–axis we obtain solutions for the different velocity components, with $\omega_{ce} = eB/m_e$ we obtain:

$$\begin{aligned} v_x &= \frac{-ie}{\omega m_e}\frac{1}{1-\omega_{ce}^2/\omega^2}\left(E_x - \frac{i\omega_{ce}}{\omega}E_y\right) \\ v_y &= \frac{-ie}{\omega m_e}\frac{1}{1-\omega_{ce}^2/\omega^2}\left(E_y + \frac{i\omega_{ce}}{\omega}E_x\right) \\ v_z &= \frac{-ie}{\omega m_e}E_z \end{aligned} \quad (9)$$

The conductivity tensor can then be written as

$$\begin{aligned} \sigma &= \frac{in_e e^2}{\omega m_e}\frac{1}{1-\omega_{ce}^2/\omega^2} \\ &\times \begin{bmatrix} 1 & -i\omega_{ce}/\omega & 0 \\ i\omega_{ce}/\omega & 1 & 0 \\ 0 & 0 & 1-\omega_{ce}^2/\omega^2 \end{bmatrix} \end{aligned} \quad (10)$$

Inserting σ and Eq. 6 for the dielectric tensor in the dispersion relation 5 we can solve the determinant for the refractive index N and obtain the *Appleton–Hartree* equation

$$\begin{aligned} N^2 &= 1 - \frac{A\cdot(1-A)}{1-A-1/2B^2 sin^2\theta \pm C} \quad (11) \\ A &= \frac{\omega_{pe}^2}{\omega^2} \quad ; \quad B = \frac{\omega_{ce}}{\omega} \\ C &= \left[\left(1/2B^2 sin^2\theta\right)^2 + \left(1-A\right)^2 B^2 cos^2\theta\right]^{1/2} \\ \omega_{pe} &= \sqrt{\frac{n_e e^2}{\epsilon_0 m_e}} \quad (12) \end{aligned}$$

The angle θ denotes the angle between the wave vector and the magnetic field, ω_{pe} is the plasma frequency and n_e is the electron density. Two interesting cases can be distinguished immediately. In the case $\theta = 0$ the propagation is parallel to the magnetic field. For $\theta = \pi/2$ we have a perpendicular propagation. Furthermore for every value of the angle we will get two solutions for the refractive index depending wether **E** is parallel to the magnetic field (*O–Mode*) or perpendicular (*X–Mode*) e.g. for perpendicular propagation we get

$$\begin{aligned} O-Mode \quad N^2 &= 1 - \frac{\omega_{pe}^2}{\omega^2} \quad (13) \\ X-Mode \quad N^2 &= 1 - \frac{\omega_{pe}^2\left(\omega^2-\omega_{pe}^2\right)}{\omega^2\left(\omega^2-\omega_{pe}^2-\omega_{ce}^2\right)} \end{aligned}$$

III. INTERFEROMETRY

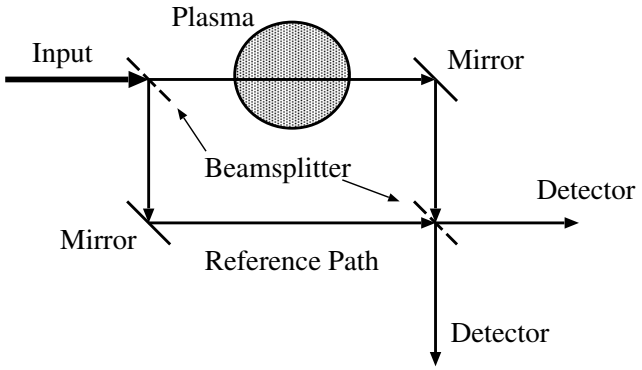

Figure 1: Schematic view of a Mach–Zehnder Interferometer

A standard tool for measuring the electron density n_e within a plasma is an interferometer. In this case we have the refractive index for *O–Mode* will be investigated with the assumption that $\omega_{ce}/\omega \ll 1$ neglecting the effects of the magnetic field. The measurement of the electron density is done by comparing the phase change of two waves, one traveling through the plasma, and another reference wave traveling through vacuum or air. The phase change is then given by

$$\Delta\Phi = \int kdl = \int (N-1)\frac{\omega}{c}dl \quad (14)$$

The above equation can be rewritten with the use of the critical electron density n_c which is reached when the wave is in cut–off corresponding to $N = 0$. From Eq. 13 we achieve the critical density as

$$n_c = \frac{\epsilon_0 m_e \omega^2}{e^2} \quad (15)$$

yielding for the phase change:

$$\begin{aligned} \Delta\Phi &= \frac{\omega}{c}\int\left(\sqrt{1-\frac{n_e}{n_c}}-1\right)dl \\ &= \frac{\omega}{2cn_c}\cdot\int n_e dl \quad (16) \end{aligned}$$

where we have assumed that $n_e \ll n_c$.
Several types of interferometers exist. Two arm interferometer like *Michelson Interferometer* or *Mach-Zehnder-Interferometer* (Fig. 1) and multiple beam interferometer as *Fabry–Perot–Interferometer*.
The major difference between the Michelson– and the Mach–Zehnder–Interferometer is the fact that the reference as well as the plasma path are only traveled once in the Mach–Zehnder set–up. Two major drawbacks of all those types of interferometer are

- The ambiguity of phase changes for $\Delta\Phi = n\cdot\pi$

- Amplitude variations due to refraction or absorption of the beam

To overcome those problems the frequency of the reference wave is shifted with a rotating grating. The detector will mix the two incoming frequencies and yield an intermediate frequency $\Delta\omega_0 = \omega_1 - \omega_2$ and higher harmonics. The frequency ω_2 is the modulated frequency. Such a detection method is called a heterodyne receiver. An additional phase change due to the plasma yield $\Delta\omega = \Delta\omega_0 + d\Phi/dt$. This allows a distinction between positive and negative phase change.

For interferometric measurements the wave generator has to fulfill several requirements. First of all the measurement of a radial electron density profile several channels have to be fed by one generator. Therefore the intensity of the generator has to be large enough to allow a splitting into several channels. The second requirement is the time resolution of $\Delta t = 100\mu s$ to measure fast processes in the plasma (e.g. sawtooth crash, precursor modulation). As a consequence the detector must have a large signal to noise ratio to detect even 1%–modulations of the signal. A third requirement is that the frequency of the generator is in a range where the plasma has no cut–offs or resonances. The operation range of a tokamak will give a lower limit of the used frequency. From the *O–Mode* cut–off condition (Eq. 13) and ω_{pe} the needed frequency of the generator can be estimated, assuming an upper operation limit of $n_e = 2 \times 10^{20} cm^{-3}$ yielding $f_c \approx 126GHz$. To have a small angular deviation of the beam ($\Delta\alpha \leq 10mrad$) the frequency must fullfill the condition $f \geq 5f_c$.

In the desired frequency region klystrons or BWO's cannot be used as intensive power source since the output power is only in the order of several mW. However molecule laser offer enough intensity [2]. Specially the *HCN–, ($\lambda = 337\mu m$)* and *DCN–, ($\lambda = 190\mu m$)* laser yield $P_{out} \approx 200 - 250mW$.

As can be seen from Eq. 16 the interferometric phase shift is integrated along the line of sight. Of more importance is the local electron density and the profile of the local density. To fulfill an accurate calculation of the local density from the phase shift tomographic methods have to be used. Therefore the phase shift has to be measured within a poloidal cut of the tokamak at several chords at different radial position. In medical services such tomographic reconstructions are performed with 100 and more chords. However in high temperature plasma physics only a few chords can be realized. Therefore assumption about the shape and symmetry of the plasma have to be made. With a mathematical inversion procedure called *Abel–Inversion* a density profile is calculated. A disadvantage of the previous mentioned short wavelength are the possible vibrations of the interferometer frame. Already small vibrations yield a disturbance of the path length and therefore an error in the phase measurement. To overcome this problems (i) the optics has to be mounted in a rigid frame or (ii) two different wavelength can be used. The shorter wavelength measures the disturbance of the diagnostic and the longer wavelength measures the refractive effects due to the plasma. In more sophisticated experiments it is even possible to detect the disturbance of the path length and try to adjust the pathlength by a moving mirror. Another problem is the bending of the chords. The plasma acts itself as a lens. Specially in the case of steep density gradients at the plasma boundary the changes in the refractive index will be quite large. As a consequence the optical path length will increase and yield larger phase delays or the deviation will result in a loss of signal. The inversion procedure will result in density profiles with higher edge densities and smaller one in the plasma center. The angular deviation of the beam with respect to the incident beam can be estimated assuming a chord parallel to the z–axis crossing the plasma and a refractive index changing along the z–axis. The deviation of the chord along the perpendicular y–axis can be expressed by the angle θ between

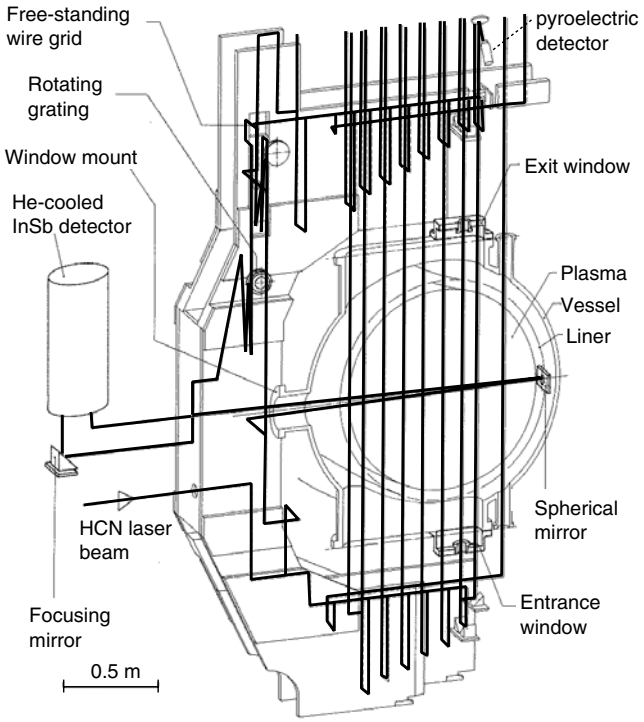

Figure 2: Schematic view of the nine channel HCN–interferometer–polarimeter installed at TEXTOR. The thick lines show the optical path of the nine vertical, the horizontal and the reference channels.

the chord and the z–axis and is calculated by

$$\theta = \frac{d}{dy}\int N dl = \frac{\lambda}{2\pi}\frac{d\Phi}{dy} \qquad (17)$$

At TEXTOR a interferometer–polarimeter of Mach-Zehnder type [3] using a HCN-laser is installed. The system consists of nine channels, distributed across the minor radius of the tokamak and a reference channel, shown on the left side of the vessel in Fig. 2. In addition one horizontal channel is installed. The signals are detected by pyroelectric detectors and the horizontal channel by He–cooled InSb detector.

IV. POLARIMETRY

Due to the magnetic field the refractive index is different for the two circular components of a linear polarized incident wave. In the case of a plasma current, generating a poloidal magnetic field, the interferometer–polarimeter set–up shown in Fig. 2 is sensitive to the parallel component of the poloidal magnetic field. For a propagation of the wave parallel ($\theta = 0^o$) to the magnetic field component, the refractive index can be achieved from Eq. 11 retaining only first order terms in B, then we get:

$$N^2 \approx 1 - A \pm AB cos\theta \qquad (18)$$

Since ordinary and extraordinary waves have different refractive indices a difference in phase change will be measured. This difference in the phase change, causes a rotation of the electric field vector of a linearly polarized wave (*Faraday Rotation*). This is a rotation of the polarization plane. The phase change along the z–axis is given by:

$$\Delta\Phi = \frac{\omega}{c}\ (N_+ - N_-)\ z \qquad (19)$$

The Faraday rotation angle α can be expressed by the measured phase change and making use of Eq. 18 where only the first order terms in ω_{ce}/ω are considered.

$$\begin{aligned}\alpha &= \frac{\Delta\Phi}{2} = \frac{e}{2\ m_e\ c}\int \frac{n_e\ \mathbf{B}\cdot\mathbf{dl}}{n_e\,(1\ -\ n_e/n_c)^{1/2}} \\ &\approx \frac{e}{2\ m_e\ c}\int \frac{1}{n_c}\cdot n_e \mathbf{B}\cdot\mathbf{dl} \qquad (20)\end{aligned}$$

This last approximation is valid if the ratio of electron density to critical density is less than one. With the measurement of α the poloidal magnetic field can be estimated. The approximation is only depending on n_c which itself is a function of the used wavelength an the magnetic field, so that a numerical approach can be expressed by

$$\begin{aligned}\alpha\,[degree/cm] &= 1.5\times10^{-17}\ \lambda^2\,[mm] \\ &\times\ n_e\left[cm^{-3}\right]\ B\,[Gauss] \qquad (21)\end{aligned}$$

After the measurement of the poloidal magnetic field at different radial positions the current profile j as well as the q-profile can be estimated.

V. REFLECTOMETRY

As most of the microwave diagnostic the reflectometry is a not a space consuming diagnostic and due to the small power levels (several mW) it will not perturb the plasma. The diagnostic potential of the reflectometry [4] is the measurement of a density profile and the measurement of small scale density fluctuations as well as MHD–Modes. Concerning its accuracy the radial resolution is in the range of $\Delta r \leq 0.5cm$. Reflectometry is therefore a good tool for plasma edge density measurements [5].
The principle of reflectometry is the measurement of the phase change of an launched microwave travelling through the plasma with a reference wave travelling through a piece of wave guide. The microwave is reflected at a special density layer where the refractive index becomes zero. The phase change can be calculated by Eq. 22, where c denotes the speed of light and $N_{X,O}$ the refractive index as calculated from Eq. 13.

$$\Phi = \frac{2\omega}{c}\int_{R_{edge}}^{R_{cut-off}} N_{X,O}(R,\omega)dR - \frac{\pi}{2} \qquad (22)$$

At the reflection layer itself a phase jump of $\pi/2$ will arise. The refractive index depends on the polarisation of the launched microwave (selected by the orientation of the launching and recieving antenna). Reflectometry can be done in *O–Mode* and *X–Mode* respectively. Using *X–Mode* relectometry has the advantage of $\omega_{cut-off} > 0$ for $n_e(r) = 0$. However in this case N_X depends on the B_T which is not the case for *O–Mode* reflectometry. Another advantage of *X–Mode* reflectometry is the larger access in the radial range of the density profile. With *O–mode* reflectometry only half of the profile can be measured, since a reflectometer can not look behind the horizon.
The determination of the density profile was somewhat difficult in the past due to the large sweep times of the available microwave generators. The sweep time of the generators should be $\tau_{sweep} \leq \tau_{fluc}$, where τ_{fluc} is the life time of the fluctuation. Today's technique allows a sweep time of $10\mu s$ using hyperabrupt varactor tuned oscillators (HTO). In this case the fluctuations

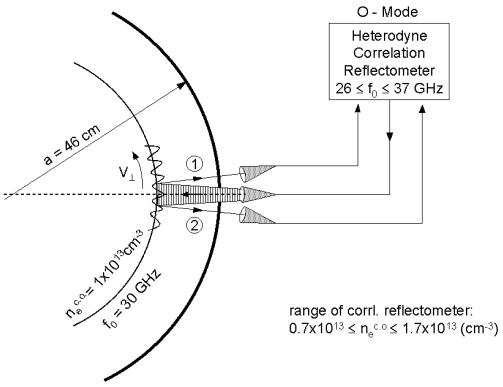

Figure 3: Schematic view and principal of the measurement of the heterodyne correlation reflectometer at TEXTOR

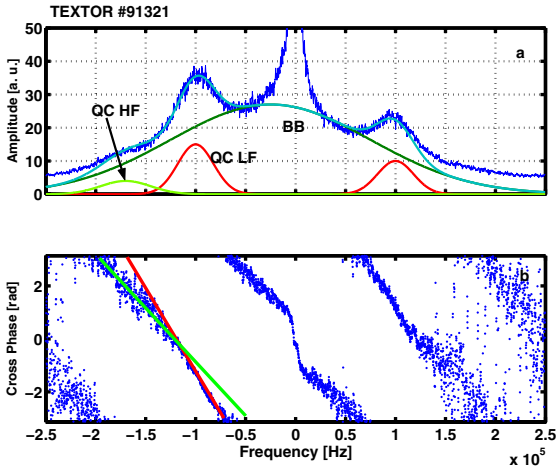

Figure 4: (**a**) Amplitude spectrum obtained from reflectometry showing the different fluctuation components. (**b**) The different propagation velocities are determined from the slopes in the cross phase spectrum.

are frozen during one sweep of the oscillator.

With a heterodyne correlation reflectometer one is able to observe radially and poloidally resolved fluctuations. On TEXTOR such a reflectometer is installed within the frequency range of $26 \leq f \leq 36GHz$. The principle of this reflectometer are shown in Fig. 3. The central antenna launches the microwave and the reflected signal is observed via one antenna on the top and bottom. From the cross correlation the propagation time of the fluctuations on a density layer can be measured [6]. This can be done for different plasma regimes and heating scenarios. In Fig. 4. shows the amplitude and cross phase spectra deduced from the quadrature dectors of the reflectometer. From the amplitude spectrum different fluctuations can be recognised. Most pronounced are broad band fluctuations and the quasi coherent modes at low and high frequency. The different propagation velocities of the quasi coherent mode are obvious from the different slopes in the cross phase spectrum. It is possible from these measurements to get information on the underlying transport models.

VI. ECE DIAGNOSTIC

Up to now only those techniques were discussed, launching a microwave into the plasma. Now the properties of the radiation emitted by the plasma are investigated. The radiation emitted by the gyrating electrons is called the electron cyclotron radiation ω_{ce},

$$\omega_{ce} = \frac{e \cdot B}{m_e \cdot \gamma} \tag{23}$$

where γ is the relativistic mass factor. Due to relativistic effects the radiation is emitted also in higher harmonics of ω_{ce}. Having a spatial varying toroidal magnetic field as in a tokamak where $B_t \propto 1/R$ a relation between the emitted frequency and the location within the plasma is possible. In the case of a maxwellian energy distribution of the electrons the intensity of the emitted radiation can be related to the temperature. The emitted frequency spectrum can be discribed by Planck's equation. Since in a fusion plasma $\hbar\omega \ll kT_e$ the Rayleigh–Jeans approximation can be used.

$$I(\omega) = B(\omega) = \frac{\omega^2 \cdot T_e}{8 \cdot \pi^3 \cdot c^2} \tag{24}$$

The measurement of the intensity of the emitted frequency alone is not sufficient. Also the transport of the radiation from its point of emission within the plasma to the observing antenna has to be taken into account. The transport of the radiation is described by

$$\frac{dI}{ds} = j(\omega) - I \cdot \alpha(\omega) \tag{25}$$

where s is the ray path and α the absorption coefficient and j the emissivity which are itself a functions of the frequency. The differential equation can be integrated yielding

$$I(s_2) = I(s_1) \cdot e^{-\tau_{21}} + \frac{j}{\alpha} \cdot [1 - e^{-\tau_{21}}], \quad \tau_{21} = \tau_2 - \tau_1 \tag{26}$$

where τ is the optical depth

$$\tau = \int \alpha(\omega) ds \tag{27}$$

The absorption coefficient is itself a function of the local plasma parameters as n_e and T_e and from the polarization of the wave (e.g. *X– or O–Mode*) and the harmonic

number. For practical use it is more convenient of finding an equation for τ. For X-mode observation and perpendicular propagation $\theta = 90^o$ τ can be calculated from a WKB approach by [7]

$$\tau_m^X = \frac{\pi \cdot m^{2(m-1)}}{2^m \cdot (m-1)!} \cdot \left(\frac{\omega_{pe}}{\omega_{ce}}\right)^2 \cdot \left(\frac{T_e}{m_e c^2}\right)^{(m-1)} \cdot \frac{\omega_{ce} R}{c} \times \left[N_\perp^{(X)}\right]^{2m-3} \cdot \left[1 + \frac{\left(\omega_{pe}/\omega_{ce}\right)^2}{m\left[m^2 - 1 - \left(\omega_{pe}/\omega_{ce}\right)^2\right]}\right]^2 \quad (28)$$

with

$$\left[N_\perp^{(X)}\right]^2 = 1 - \left(\frac{\omega_{pe}}{m\omega_{ce}}\right)^2 \cdot \frac{\left[m^2 - \left(\omega_{pe}/\omega_{ce}\right)^2\right]}{\left[m^2 - \left(\omega_{pe}/\omega_{ce}\right)^2\right] - 1/2} \quad (29)$$

where m denotes the harmonic number and R is the major radius of the tokamak.
For optical thick plasmas ($\tau \gg 1$) the first term on the right side of Eq. 26 becomes small, yielding:

$$T_e^{rad} = \frac{\omega^2 \cdot T_e}{8 \cdot \pi^3 \cdot c^2} \cdot \left(1 - e^{-\tau}\right) \quad (30)$$

Another problem connected with the propagation of electron cyclotron radiation in the plasma are resonances and cut–offs. To find those positions we start from the *Appleton–Hartree relation* (Eq. 11) again. As already known from the first section the refractive index can be used to calculate the cut–off and the absorption frequencies for the propagation in *X–Mode*. Cut–off and resonances are depending on the local B– and n_e–values. For $N^2 = 0$ a cut–off will reflect the wave. If $N^2 = 1$ a resonance will absorb the wave. As can be seen from the Eq. 13 for *X-Mode* propagation perpendicular to the magnetic field we get the following equation for cut–off,

$$\omega_{CO1,2} = \sqrt{\frac{\left(2\omega_{pe}^2 + \omega_{ce}^2\right)^2}{2} \pm \sqrt{\frac{\left(2\omega_{pe}^2 + \omega_{ce}^2\right)^2}{4} - \omega_{pe}^4}} \quad (31)$$

and for resonances in the plasma we get:

$$\omega = \omega_{pe} \quad (32)$$

$$\omega = \sqrt{\omega_{pe}^2 + \omega_{ce}^2} \quad (33)$$

From Fig. 5 it becomes clear that the $1st$ harmonic can not be used for ECE-measurements since $\omega_{ce} \leq \omega_{pe}$. But as long as the n_e is small enough the $2nd$ harmonic is very well suited to measure the electron temperature. However for an increased density the lower cut–off frequency overcomes the $2nd$ harmonic. Already when the local n_e reaches $80-85\%$ of the cut–off density the $2nd$ harmonic intensity drops, because of the divergence of the antenna beam [8]. In this case the $3rd$ harmonic must be used. In Fig. 6 the behaviour of $2nd$ and $3rd$ harmonic is shown. The drop of the $2nd$ harmonic intensity at $t = 2.0s$ (80% of the cut–off density) is clearly seen. However the cut–off is reached at $t = 3.2s$. Disadvantage of this method is that the plasma is not optical thick anymore. Also multiple reflections of the radiation due to the plasma facing walls have to be taken into account. Therefore the first term in Eq. 26 is not zero and reflections from the wall have to be taken into account. The reflection coefficient ρ of the wall is material depending. For a wall covered by graphite tiles $\rho = 0.7$ is achieved [9]. The equation for the estimation of the temperature has to be modified

$$T_e^{rad} = \frac{\omega^2 \cdot T_e}{8 \cdot \pi^3 \cdot c^2} \cdot \frac{\left(1 - e^{-\tau}\right)}{1 - \rho \cdot e^{-\tau}} \quad (34)$$

To overcome the problem with reflections from the wall often tiles with a roof–top like structure are positioned on the surface on which the antenna is looking. Another complication of this method is the knowledge of the local electron density (e.g. from interferometry) and temperature when calculating the optical depth. On the other hand this method can be used to estimate the local n_e from $3rd$ harmonic when the local T_e is already estimated from the $2nd$ harmonic. The measurement of T_e from $3rd$ harmonic is restricted to a small frequency range where the frequency range of $2nd$ and $3rd$ harmonic do not overlap (see Fig. 5). Otherwise a mixture of both harmonics will be measured and yield wrong T_e–values.

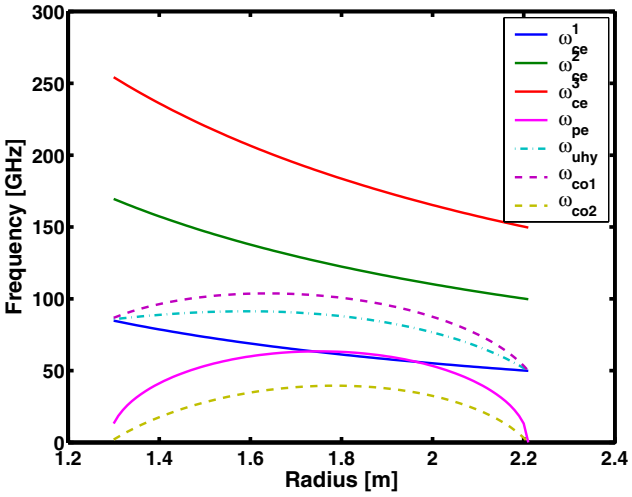

Figure 5: Cut–offs and resonances for a parabolic n_e–profile and $B_t = 2.25T$ and $n_e^{max} = 5 \cdot 10^{19} m^{-3}$. Furthermore the first three harmonics of the electron cyclotron frequency are shown

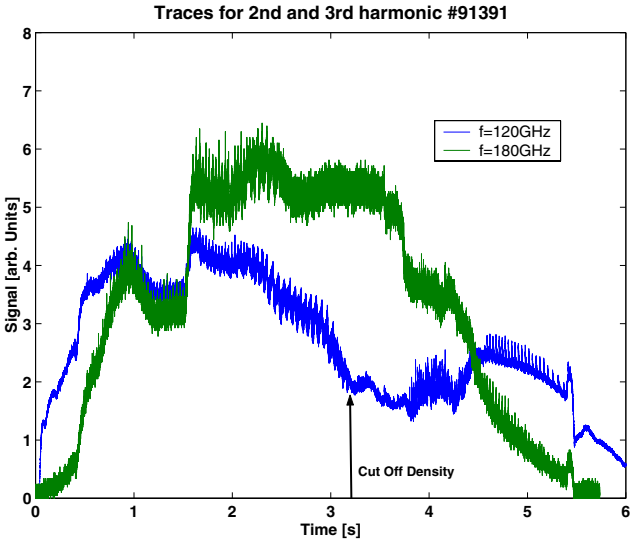

Figure 6: Temporal development of the $2nd$ and $3rd$ harmonic of the electron cyclotron radiation $f_{ce} = 60GHz$.

In devices with a low magnetic field or overdense plasmas even 3^{rd} harmonic ECE is in cut off. However temperature information can be obtained via the complex way of mode conversion. The Electron Bernstein Wave (EBW) is an electrostatic wave which is not limited by cutoffs [10]. However it cannot propagte outside the plasma. After a conversion into an electromagnetic wave it can be detected by standard heterodyne radiometers with the typical advantages as high time resolution and high sensitivity. Two different methods to obtain the electron temperature are used (i) the B–X'–X conversion and (ii) the B–X'–O conversion. Both methods use the B–X' conversion however the second conversion step is different. In the first electron Bernstein wave is converted to the slow X–mode (X') at the upper hybrid resonance (UHR). Afterwards a tunneling of the slow X–mode to the fast X–mode (X) takes place and the radiation can escape from the plasma. The radiation is observed in the equatorial plane perpendicular to the toroidal magnetic field. This method is favourable in spherical devices with low magnetic field as NSTX or CDX. The conversion efficiency depends strongly on the product of density scale length L_n and the magnetic field at the UHR. A value of $L_n \approx .005 - .01$m is necessary to achieve $\approx 100\%$ conversion efficiency at NSTX [11]. The relative narrow maximum in the diagram of the conversion coefficient versus L_n allows a maximal conversion only for a small range of plasma parameters. To overcome this problem a special limiter–antenna configuration is in use. With this technique L_n could be adjusted to give the largest possible conversion coefficient and the parameter range could be extended. However density fluctuation at the plasma edge can still influence the conversion coefficient, which could be an additional benefit of the diagnostic to detect the density fluctuation level at the plasma edge.

The second method (B–X'–O) conversion is used in the T_e-diagnostic at W7AS [12] and requires oblique ECE-observation. For this method the EBW is converted to a slow X–mode at the UHR. Due to a coincidence of the cutoffs for O– and X–mode, the ECE-radiation is observed in O–mode under oblique angles. However the large parallel velocity component yields a large Doppler shift of the spectrum. The best observation position is deduced from ray tracing calculations and was found at $\phi \approx 36^o$ with a conversion coefficient $\approx 90\%$. This method is not restricted to low toroidal magnetic field and since the conversion layer for X– to O–mode lies deeper in the plasma the conversion coefficient is not sensitive to a strongly varying L_n due to e.g. ELM's. Furthermore it is applicable over a larger range of plasma parameters.

The radiation measurement at frequencies above $f = 70GHz$ is difficult since the amplifier in this frequency range are noisy and the total amplification of the signal has to be around $80db$, due to the low input power [13]. To overcome this problem heterodyne radiometers are used for the measurement of T_e. They have a local oscillator for down conversion of the input frequency. As local oscillators Gunn-diodes made of GaAs are used because they are stable in frequency and have long lifetime compared with other microwave sources. The HF–frequency is mixed with the frequency of the local oscillator, yielding an intermediate frequency ZF. The ZF will pass a narrow filter with $\Delta f = 100 - 200MHz$. This filter is responsible for the radial resolution of the radiometer. The noise temperature of a radiometer is very low and can be below $T_{sys} \leq 1000\ ^0K$. Unfortunately it is not possible to sweep the Gunn-diode over a large frequency range with constant output power therefore a broad-band mixer is used which covers the region from $2 - 10GHz$. With a multiplexer and additional narrow bandpass filters T_e can be measured at several frequencies using only one LO-oscillator.This kind of radiometer has in general a higher noise temperature of $T_{sys} \approx 4000\ ^0K$.

In Fig. 9 the set up of the ECE-diagnostic at TEXTOR is shown. It consists out of 11 equally spaced single channel radiometers. To increase the intensity for each radioneter two antennas are used. The intensity is distributed by $3dB$ couplers. With a video bandwidth of $10kHz$ they are fast enough to detect even details within fast plasma processes e.g. sawtooth crash. Other instruments of measuring T_e are

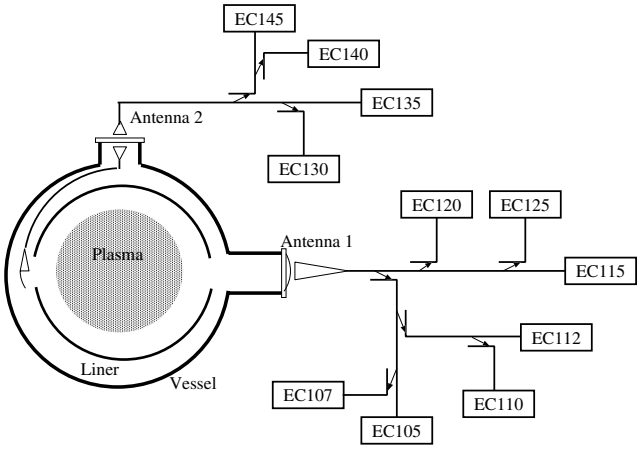

Figure 7: Set-up of the ECE–radiometers on TEXTOR. The numbers denote the frequency of the radiometer.

the Michelson–Interferometer or a grated polychromator. The Michelson–Interferometer is mostly used to measure the emitted microwave radiation over a large frequency range (e.g. $1st-4th$ harmonic). This is done by a vibrational or pneumatical mirror in the device, allowing a scan over a large frequency range within $\approx 10ms$. The interferometer measures the superposition of two amplitudes $A_{1,2}$ as function of the position x of the movable mirror. The first amplitude $A_1(\omega)$ is created by the reflection on the fixed mirror, the second one $A_2(\omega)$ is due to the reflection on the movable mirror.

$$I(x) = \int \left|A_1\left(\omega\right) + A_2\left(\omega\right)\right|^2 d\omega \qquad (35)$$

After a Fourier–transformation the spectral intensity as function of the frequency is obtained. A disadvantage of this, in principle very useful, instrument is the required cooling of the detector. Since the power transfered to detector is very small the detector noise has to be reduced as much as possible. This is done normally by cooling with liquid helium.

The calibration of the ECE diagnostic is done by using black body sources at two different temperatures e.g. liquid nitrogen and room temperature. The temperature of this sources are very low with respect to the measured temperature in a plasma. A calibrated attenuator is used to reduce the intensity during plasma operation. The calibration itself has to be done over long intervals to reduce the effect of statistical noise. If one channel is calibrated absolutely the other channels can be calibrated during plasma operation by a relative calibration during a B_t–scan.

Instead of measuring the microwave power emitted by the plasma one can think about the measurement of the transmitted fraction of the power, launched on one side of the tokamak and observed on the opposite side (*ECA–measurement*). Those measurements were performed at the RTP tokamak [14]. Together with ECE-measurements the ECA can complete the information about T_e in cases of optical thin plasmas by:

- Direct measurement of the optical thickness τ
- Since $\tau \propto n_e T_e$, ECA yields a direct measurement of the plasma pressure
- For $\tau \leq 1$ and known τ and n_e calculation of T_e

REFERENCES

1. I.H. Hutchinson, *Principles of Plasma Diagnostic*, Cambridge University Press, (1987)
2. N.C. Luhmann, *Instrumentation and Techniques for Plasma Diagnostics*, in *Infrared and Millimeter Waves*, Vol. 2, Academic Press, New York, (1979)
3. H.R. Koslowski, H. Soltwisch, *Fusion Engeneering and Design*, **34-35**, 143-150, (1995)
4. C.Laviron, A.J.H.Donne, M.E.Manso and J.Sanchez *Plasm Phys. Control. Fusion* **38** (1996) 905-936
5. F.Clairet,C.Bottereau, J.M.Chareau, M.Paume and R.Sabot *Plasma Phys. Control. Fusion* **43** (2001) 429-441
6. A.Krämer–Flecken, H.R.Koslowski, V.Dreval, S.Soldatov P4.016 *28th EPS 2001 Madeira* 18-22 June 2001
7. M. Bornatici, *Plasma Physics*, **Vol. 24**, No. 6, 629, (1982)
8. W.H.M. Clark, *Plasma Physics*, **Vol. 25**, No. 12, 1501, (1983)
9. A. Krämer–Flecken, P.C. De Vries, *Proceedings on the tenth workshop of ECE and ECRH*, p. 209, World Scientific, Singnapore, (1997)
10. A.K. Ram and S.D. Schultz, Physics of Plasmas, Vol 7, No. 10 (2000) pp 4084–4094
11. G. Taylor et al., Physics of Plasmas, Vol. 9 No. 1 pp167–170 (2002)
12. F. Volpe et al., Rev. Sci. Instrum., Vol. 74 No. 3, pp 1409–1413 (2003)
13. B. Vowinkel, *Passive Mikrowellenradiometrie*, Vieweg & Sohn, Braunschweig, 1988
14. J.F.M. van Gelder, *Electron Cyclotron Wave Absorption Experiments in Tokamak Plasma*, p. 71, PHD–Thesis University Utrecht, Utrecht (1996)